Biochemical and Biophysical Research Communications 438 (2013) 129–132

Contents lists available at ScienceDirect

Biochemical and Biophysical Research Communications

journal homepage: www.elsevier.com/locate/ybbrc

Solution structure and backbone dynamics of human Raf-1 kinase inhibitor protein

Chenyun Guo [a,1], Cuiying Yi [b,1], Yu Peng [b], Yi Wen [b], Donghai Lin [a,*]

[a] The Key Laboratory for Chemical Biology of Fujian Province, College of Chemistry and Chemical Engineering, Xiamen University, Xiamen 361005, China
[b] NMR Laboratory, Shanghai Institute of Materia Medica, Chinese Academy of Science, Shanghai 201203, China

ARTICLE INFO

Article history:
Received 10 July 2013
Available online 17 July 2013

Keywords:
Human Raf-1 kinase inhibitor protein (hRKIP)
Solution structure
Ligand-binding pocket
NMR
Model-free analysis
Protein dynamics

ABSTRACT

Human Raf-1 kinase inhibitor protein (hRKIP) is a small multi-functional protein of 187 residues. It contains a conserved pocket, which binds a wide range of ligands from various small molecules to distinct proteins. To provide a structural basis for the ligand diversity of RKIP, we herein determined the solution structure of hRKIP, and analyzed its structural dynamics. In solution, hRKIP mainly comprises two anti-parallel β sheets, two α helices and two 3_{10} helices. NMR dynamic analysis reveals that the overall structure of hRKIP is rigid, but its C-terminal helix which is close to the ligand-binding site is mobile. In addition, residues around the ligand-binding pocket exhibit significant conformational exchange on the μs–ms timescale. Conformational flexibility may allow the ligand-binding pocket and the C-terminal helix to adopt various conformations to interact with different substrates. This work may shed light on the underlying molecular mechanisms of how hRKIP recognizes and binds diverse substrate ligands.

1. Introduction

Human Raf-1 kinase inhibitor protein (hRKIP) is a member of the phosphatidylethanolamine-binding protein (PEBP) family, which was first identified by its intrinsic binding of phospholipids [1,2]. RKIP can also bind distinct kinases to regulate several important signaling pathways, including those of MAPK (mitogen-activated protein-kinase), GPCR (G-protein coupled receptor) and NF-κB (nuclear factor-kappa B) signaling [3–5]. These signaling cascades are crucial in controlling cellular growth, motility, apoptosis, genomic integrity and therapeutic resistance. Recent reports implicated that RKIP was negatively correlated with tumor growth and cancer metastasis, because its expression level decreased in many cancers, including metastatic prostate cancers [6], melanoma cancer cells [7], and breast cancer metastases [8].

Crystal structures of the RKIP proteins from various species with diverse biological functions reveal that RKIP adopts a unique topology containing a conserved ligand-binding pocket (PDB: 1BEH, 2IQX, 2QYQ). Ligands range from phospholipids to nucleotides, and to various protein kinases that modulate signal pathways [1–5,9]. So far it remains unclear how a small protein of 21 kDa co-ordinates binding of, for example, so many distinct protein kinases (Raf-1, GRK2, NIK, TAK1 and GSK3α/β), which in turn control many signaling cascades. To understand the underlying molecular mechanism of RKIP binding to diverse substrates, it is important to determine the solution structure and to analyze the structural dynamics of RKIP. Prior crystallographic analyses on apo-hRKIP and the ligand-bound RKIP complexes [9] were not able to explain substrate diversity of RKIP, because these structures are highly similar. In the present work, we determined the solution structure and analyzed backbone dynamics of hRKIP using multi-dimensional heteronuclear NMR techniques. Our results reveal the structural and dynamic characteristics of hRKIP and offer invaluable insights into the molecular mechanism of hRKIP functions.

2. Materials and methods

2.1. Sample preparation and NMR experiments

Preparation of ^{15}N- and $^{15}N/^{13}C$-labeled hRKIP, NMR experiments and data processing were performed as described previously [10].

Abbreviations: RKIP, Raf-1 kinase inhibitor protein; MAPK, mitogen-activated protein kinase; GPCR, G-protein coupled receptor; NF-κB, nuclear factor-kappa B; GTP, guanosine tri-phosphate; GDP, guanosine di-phosphate; FMN, flavin mono-nucleotide; PE, o-phosphorylethanolamine; NOE, nuclear overhauser effect; NOESY, nuclear overhauser enhancement spectroscopy; HSQC, heteronuclear singular quantum correlation; R_1, longitudinal relaxation rate; R_2, transverse relaxation rate; RMSD, root-mean-square deviation; S^2, order parameters; R_{ex}, conformational exchange rate.

* Corresponding author. Fax: +86 592 2186078.
E-mail address: dhlin@xmu.edu.cn (D. Lin).
[1] These authors contributed equally to this work.

0006-291X/$ - see front matter © 2013 Elsevier Inc. All rights reserved.
http://dx.doi.org/10.1016/j.bbrc.2013.07.039

2.2. Structure calculation and refinement

The NOE (Nuclear Overhauser Effect)-derived distance restraints were obtained from 3D ^{13}C-edited NOESY-HSQC (100 ms mixing time) and 3D ^{15}N-edited NOESY-HSQC (100 ms mixing time). Backbone dihedral angle restraints (Ψ and Φ) were calculated using the TALOS program [11] based on $^{13}C_{\alpha}$, $^{13}C_{\beta}$, $^{13}C'$ and ^{15}N chemical shifts. The three-dimensional structures were calculated using ARIA2.2 [12] and CNS1.2 [13] with a modified simulated annealing protocol [14]. A family of 200 structures was calculated. Twenty lowest energy structures were selected and further refined with water. The PROCHECK-NMR [15] and WHATIF [16] programs were used to evaluate the quality of the structures (Table 1).

2.3. Backbone ^{15}N relaxation measurements

A complete set of backbone amide longitudinal relaxation rate (R_1), transverse relaxation rate (R_2) and ^{1}H–^{15}N NOE relaxation data sets were acquired on a Varian Unity Inova 600 MHz spectrometer. ^{15}N T_1 values were measured from 2D ^{1}H–^{15}N HSQC spectra recorded with relaxation delays of 10.83, 54.17, 108.34, 216.68, 325.02, 541.70, 866.72, 1191.74, 1570.93 and 1950.12 ms. ^{15}N T_2 values were determined with relaxation delays of 15.62, 31.23, 46.85, 62.46, 78.08, 93.70, 109.31, 124.93, 140.54 and 156.16 ms. ^{1}H–^{15}N steady-state NOEs were obtained by recording spectra with and without ^{1}H presaturation of 3 s duration plus a 2 s relaxation delay at 600 MHz. Both the longitudinal and transverse relaxation rates were determined by fitting the cross-peak intensities as a function of the delay to a single-exponential decay through the standard routines incorporated in the Sparky program [17]. The program Tensor2 [18] was used to analyze backbone ^{15}N relaxation parameters and perform the model-free analysis from relaxation rate R_1, R_2 and {^{1}H}–^{15}N NOE. Only residues in secondary structure elements were used for determining the overall tumbling correlation time.

Table 1
Structural statistics for the 20 lowest energy structures of hRKIP.

A. Restraints used for structure calculation	
Total unambiguous distance restraints	2480
Intra residual ($i-j=0$)	1277
Sequential ($\|i-j\|=1$)	511
Short ($2 \leqslant \|i-j\| \leqslant 3$)	132
Medium ($4 \leqslant \|i-j\| \leqslant 5$)	47
Long range ($\|i-j\| \geqslant 5$)	513
Total number of dihedral angle restraints	173
B. RMSD deviation from mean structure (Å)	
Backbone, 2nd structure	0.47 (±0.05)
Heavy atoms, 2nd structure	0.98 (±0.09)
Backbone, all atoms	0.60 (±0.06)
Heavy atoms, all atoms	1.09 (±0.09)
C. Energies (kcal/mol)	
Total	−6958.6 (±138.7)
Van der waals	−1746.3 (±41.0)
Electrostatic	−7305.64 (±111.46)
D. Violations	
NOE violation (>0.5 Å)	0
Torsion angle violation (>5°)	0
E. Ramachandran statistics	
Residues in most favored region	77.8%
Residues in allowed regions	20.6%
Residues in generously allowed region	1.2%
Residues in disallowed region	0.4%

2.4. Coordinate and data deposition

The atomic coordinates for an ensemble of 20 structures that represent the solution structure of human RKIP together with the list of restraints used for the structure calculation have been deposited in the Protein Data Bank (accession code: 2L7W).

3. Results and discussion

3.1. Solution structure of hRKIP

An ensemble of 20 lowest energy structures was determined on the basis of 2480 unambiguous distance restraints (Table 1, Fig. 1A). No distance restraint violations greater than 0.5 Å and no torsion angle restraint violations above 5° were observed in the 20 lowest energy structures. For the regular secondary structures, the average RMSD (root-mean-square deviation) value among the 20 lowest energy structures is 0.47 ± 0.05 Å for backbone atoms and 0.98 ± 0.09 Å for heavy atoms. Ramachandran plot analysis of the 20 lowest energy structures indicates that 98.4% of residues are located in the allowed regions.

The solution structure of hRKIP consists mainly of two antiparallel β sheets, two α helices and two 3_{10} helices (Fig. 1B), which is similar to its crystal structure (PDB: 1BD9). Superposition of all the backbone atoms of hRKIP residues between the crystal structure and the solution structure gives an RMSD of 1.2 Å (Fig. 1C). Similarly to the situation in the previously determined mammalian RKIP structures (PDB: 1BD9, 1B7A, 2IQY), a ligand-binding pocket is located close to the surface of hRKIP, comprising the residues on the C-terminal helix and loops of the highly conserved regions T64-N94 and P111-L123 (Fig. 1B). Moreover, the solution structure of hRKIP shows that the ligand-binding pocket is stabilized by three salt bridges between D70-H118, D72-R119 and D78-K80. In addition, the previous work demonstrates that two *cis* peptide bonds exit in the rim of the ligand-binding pocket, including the *cis* P74 located at the highly conserved DPDXP motif, and the nonproyl *cis* peptide bond located between R82 and E83 [9]. Our work suggests that the specific *cis* configuration is responsible for the strong NOE signals between the Hα atoms of A73 and P74, and those between the Hα atoms of R82 and E83 in the 3D ^{13}C-edited NOESY-HSQC spectra.

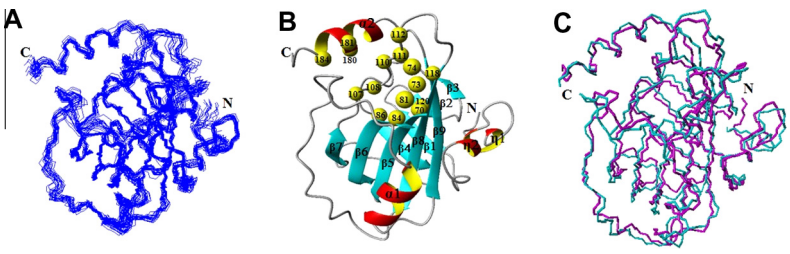

Fig. 1. NMR structure of hRKIP. (A) Superposition of the final 20 lowest energy structures. (B) Ribbon representation of the mean structure of hRKIP highlighted with secondary structures of alpha helix (α), beta strand (β), and 3_{10} helix (η). Residues located in the ligand-binding pocket are shown as yellow balls. (C) Superimposing the backbone atoms of the solution structure (magenta, PDB: 2L7W) and the crystal structure (cyan, PDB: 1BD9) of hRKIP in stereoview. (For interpretation of the references to color in this figure legend, the reader is referred to the web version of this article.)

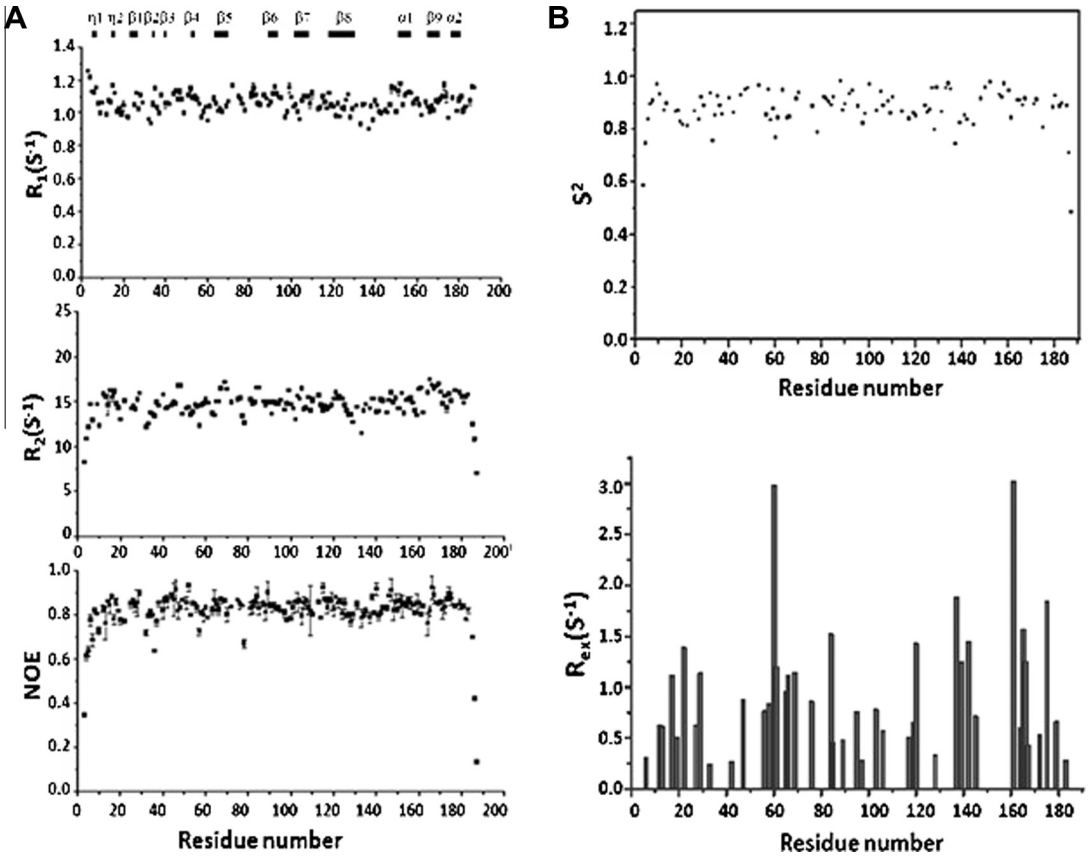

Fig. 2. Backbone dynamics analysis of hRKIP. (A) Relaxation rates R_1, R_2 and ^{1}H-^{15}N heteronuclear NOEs verse residue number. (B) The plots of the order parameter S^2 (upper), and the conformational exchange rate R_{ex} (lower) versus the residue number of hRKIP. (For interpretation of the references to color in this figure legend, the reader is referred to the web version of this article.)

3.2. Relaxation rates R_1, R_2 and heteronuclear NOEs

NMR relaxation rates R_1, R_2 and ^{1}H–^{15}N NOE values of backbone amide groups are influenced by local internal motions on ps–ns and μs–ms time scales, respectively [19]. In addition, the R_2 rates are usually contributed significantly by conformational exchange on the μs–ms time scale. Thus, analysis of the R_1, R_2, and ^{1}H–^{15}N NOE values may provide important information on protein internal motions on ps–ns and μs–ms time scales.

To analyze the backbone dynamics of hRKIP, we performed ^{15}N relaxation measurements using NMR spectroscopy. Totally, 157 assigned residues were used except the residues with overlapping signals that were not suitable for analysis. The relaxation rates R_1, R_2 and heteronuclear NOEs versus residue number are shown in Fig. 2A. The average values of R_1, R_2 and ^{1}H-^{15}N NOE are 1.06 ± 0.01 s^{-1}, 14.57 ± 0.12 s^{-1}, and 0.82 ± 0.02 s^{-1}, respectively. The R_1 values do not differ significantly among all the residues, ranging mostly between 0.9 and 1.3 s^{-1}. In contrast, the R_2 values vary considerably, ranging from 6.9 to 17.4 s^{-1}. Residues with large R_2 values include A165 (17.4 s^{-1}) and T69 (17.1 s^{-1}), suggesting conformational exchange on the μs–ms time scale. Except for the extreme N- and C-termini, most NOE values exceed 0.8, indicating that the overall structure of hRKIP is rigid. Local structural flexibility was observed in the regions of Q20-Q22, A32-V34 and G57-G61 because the NOE values of these residues are smaller than 0.8.

3.3. Model-free analysis

Analysis of the relaxation data of hRKIP in the ordered regions yielded an apparent rotational correlation time τ_m (11.5 ± 0.1 ns),

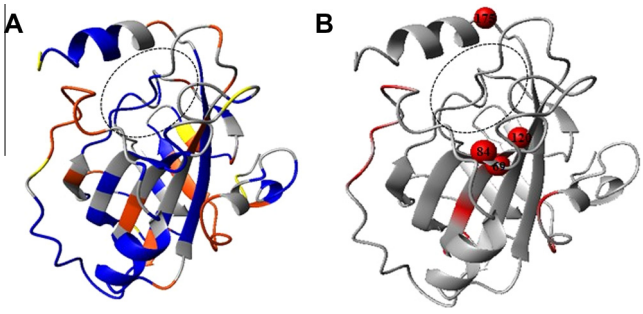

Fig. 3. Residues with S^2 and high R_{ex} are mapped onto the solution structure of hRKIP respectively (A: S^2; B: R_{ex}). Yellow: $S^2 < 0.8$; orange: $0.8 \leqslant S^2 < 0.9$; blue: $S^2 \geqslant 0.9$; gray: S^2 unavailable due to either the absence of NMR data or inability in NMR data fitting. The residues with $R_{ex} > 1.0$ are shown as red, and those located in or near the ligand-binding pocket are shown as balls. The dashed circle represents the ligand-binding pocket. The ribbon graph was generated using MOLMOL. (For interpretation of the references to color in this figure legend, the reader is referred to the web version of this article.)

corresponding to the expected value for a well-structured monomeric protein of 21 kDa. The initial rotational diffusion model derived from the relaxation data is an axially symmetric model with $D_{//}/D_{\perp}$ ratio of 1.20 ± 0.01, which is suitable for model-free analysis.

The generalized order parameter (S^2) reflects the motional restriction of the amide N—H bond vector on the ps–ns time scale, indicating the fast internal motion relative to the overall rotational diffusion. Large conformational exchange rates (R_{ex}) are usually used to identify residues experiencing significant conformational

exchange on the μs–ms time scale. The calculated S^2 and R_{ex} versus residue number were plotted in Fig. 2B. The average of S^2 value is 0.88, indicating that the overall structure of hRKIP is highly rigid, and consistent with the NOE analysis. The S^2 values for residues involved in secondary structure elements are relatively large (mean value, 0.92), except for those in the β2 strand (A33-V34, 0.81). Higher S^2 values were also observed for fragments S9-G10 (0.956), D35-E36 (0.91), D105-G110 (0.91), Q127-E135 (0.93), indicating that the conformational flexibility in these regions is very restricted. In addition to the random coils at the N- and C-termini, low S^2 values were observed for fragments E19-Q22 (0.82), A33-V34 (0.81), L58-G61 (0.83), I137-H145 (0.81), suggesting that these regions are structurally flexible (Fig. 3A). Residues with $R_{ex} > 1.0\ s^{-1}$ are mostly located on the loops comprising V17, Q22, Y29; S60, G61; I137, S139, S142; R161, and D175, suggesting structural mobility of these loops. Interestingly, residues (L66, T69, W84, Y120) located in the highly conserved β sheet also have high R_{ex} values ($>1.0\ s^{-1}$), suggesting local structural flexibility, which is in contrast with the expected structural stability associated with secondary structure (Fig. 3B).

3.4. Dynamic characteristics of the ligand-binding pocket

To provide a structural basis for the substrate diversity of hRKIP, we analyzed structural dynamics of the residues comprising the ligand-binding pocket. Residues D70, Y81, G108, G110 and L180 show relatively high S^2 value ($S^2 > 0.9$), indicating the well-ordered nature of the ligand-binding site (Fig. 3A). However, residues T69, W84 and Y120 located at the bottom of the ligand-binding pocket have large R_{ex} values (1.14, 1.52 and 1.42 s^{-1}, respectively), suggesting significant conformational exchange on the μs–ms time scale. Notably, D175 located on the loop (E172-D175) linking the β9 strand (A165-A171) and the C-terminal helix (Y176-Q183) shows a large R_{ex} value (1.84 s^{-1}). The high conformational flexibility suggests a role of D175 in positioning the C-terminal helix to, for example, control ligand access to the binding site (Fig. 3B). These dynamic findings indicate that the ligand-binding pocket undergoes significant conformational exchange on the μs–ms time scale. Since substrates of RKIP, albeit their structural diversity, share the same ligand-binding site, we propose that the observed slow internal motions (on the μs–ms time scale) associated with the ligand-binding site allow RKIP to adopt different conformations to accommodate diverse substrates.

Acknowledgments

We would like to thank Prof. L. Chen of Indiana University for editing the manuscript and discussion. This work was supported by the Chinese National Science Foundation (Nos. 30900233, 31170717, 91129713) and Natural Science Foundation of Fujian Province (No. 2011J01246).

References

[1] I. Bernier, P. Jolles, Purification and characterization of a basic 23 kDa cytosolic protein from bovine brain, Biochim. Biophys. Acta 790 (1984) 174–181.
[2] I. Bernier, J.P. Tresca, P. Jolles, Ligand-binding studies with a 23 kDa protein purified from bovine brain cytosol, Biochim. Biophys. Acta 871 (1986) 19–23.
[3] K. Yeung, T. Seitz, S. Li, P. Janoschk, B. McFerrank, C. Kaiser, F. Feek, K. Katsanakisk, D. Rose, H. Mischak, J. Sedivy, W. Kolch, Suppression of Raf-1 kinase activity and MAP kinase signalling by RKIP, Nature 401 (1999) 173–177.
[4] K. Yeung, P. Janosch, B. McFerran, D.W. Rose, H. Mischak, J.M. Sedivy, W. Kolch, Mechanism of suppression of the Raf/MEK/extracellular signal-regulated kinase pathway by the Raf kinase inhibitor protein, Mol. Cell. Biol. 20 (2000) 3079–3085.
[5] K.C. Yeung, D.W. Rose, A.S. Dhillon, D. Yaros, M. Gustafsson, D. Chatterjee, B. McFerran, J. Wyche, W. Kolch, J.M. Sedivy, Raf kinase inhibitor protein interacts with NF-kappaB-inducing kinase and TAK1 and inhibits NF-kappaB activation, Mol. Cell. Biol. 21 (2001) 7207–7217.
[6] Z. Fu, P.C. Smith, L. Zhang, M.A. Rubin, R.L. Dunn, Z. Yao, E.T. Keller, Effects of Raf kinase inhibitor protein expression on suppression of prostate cancer metastasis, J. Natl. Cancer Inst. 95 (2003) 878–889.
[7] S. Park, M.L. Yeung, S. Beach, J.M. Shields, K.C. Yeung, RKIP downregulates B-Raf kinase activity in melanoma cancer cells, Oncogene 24 (2005) 3535–3540.
[8] S. Hagan, F. Al-Mulla, E. Mallon, K. Oien, R. Ferrier, B. Gusterson, J.J. García, W. Kolch, Reduction of Raf-1 kinase inhibitor protein expression correlates with breast cancer metastasis, Clin. Cancer Res. 11 (2005) 7392–7397.
[9] M.J. Banfield, J.J. Barker, A.C. Perry, R.L. Brady, Function from structure? The crystal structure of human phosphatidylethanolamine-binding protein suggests a role in membrane signal transduction, Structure 6 (1998) 1245–1254.
[10] C. Yi, Y. Peng, C. Guo, D. Lin, ^{1}H, ^{13}C, ^{15}N backbone and side-chain resonance assignments of the human Raf-1 kinase inhibitor protein, Biomol. NMR Assign. 4 (2010) 1–4.
[11] G. Cornilescu, F. Delaglio, A. Bax, Protein backbone angle restraints from searching a database for chemical shift and sequence homology, J. Biomol. NMR 13 (1999) 289–302.
[12] W. Rieping, M. Habeck, B. Bardiaux, A. Bernard, T.E. Malliavin, M. Nilges, ARIA2: automated NOE assignment and data integration in NMR structure calculation, Bioinformatics 23 (2007) 381–382.
[13] A.T. Brunger, Version 1.2 of the Crystallography and NMR system, Nat. Protoc. 2 (2007) 2728–2733.
[14] M. Fossi, H. Oschkinat, M. Nilges, L.J. Ball, Quantitative study of the effects of chemical shift tolerances and rates of SA cooling on structure calculation from automatically assigned NOE data, J. Magn. Reson. 175 (2005) 92–102.
[15] R.A. Laskowski, J.A. Rullmannn, M.W. MacArthur, R. Kaptein, J.M. Thornton, AQUA and PROCHECK-NMR: programs for checking the quality of protein structures solved by NMR, J. Biomol. NMR 8 (1996) 477–486.
[16] G. Vriend, WHAT IF: a molecular modeling and drug design program, J. Mol. Graph. 8 (1990) 52–56.
[17] T.D. Goddard, D.G. Kneller. <http://www.cgl.ucsf.edu/home/sparky>.
[18] P. Dosset, J.C. Hus, M. Blackledge, D. Marion, Efficient analysis of macromolecular rotational diffusion from heteronuclear relaxation data, J. Biomol. NMR 16 (2000) 23–28.
[19] A.G. Palmer III, Dynamic properties of proteins from NMR spectroscopy, Curr. Opin. Biotechnol. 4 (1993) 385–391.